Serb. Astron. J. № 195 (2017), 9 - 21 **UDC 524.7 NGC1023, NGC4526**
DOI: https://doi.org/10.2298/SAJ170330006S Original scientific paper

DYNAMICAL MODELS OF TWO LENTICULAR GALAXIES: NGC 1023 AND NGC 4526

S. Samurović

Astronomical Observatory, Volgina 7, 11060 Belgrade 38, Serbia
E–mail: *srdjan@aob.rs*

(Received: March 30, 2017; Accepted: July 1, 2017)

SUMMARY: We study kinematics and dynamics of two lenticular galaxies that possess globular clusters (GCs) which extend beyond approximately seven effective radii. We analyze two nearby lenticular galaxies, NGC 1023 and NGC 4526, based on their GCs. We extract the kinematics of these galaxies and use it for dynamical modeling based on the Jeans equation. The Jeans equation was solved in both the Newtonian mass-follows-light approach assuming constant mass-to-light ratio and assuming a dark halo in the Navarro-Frenk-White form. We find that while the first galaxy, NGC 1023, does not need a significant amount of dark matter, in the other galaxy, NGC 4526, the dark component fully dominates stellar matter in the total dynamical mass. In this paper we also used three different MOND approaches and found that while for both galaxies MOND models can provide successful fits of the observed velocity dispersion, in the case of NGC 4526 we have a hint of an additional dark component even in the MOND framework.

Key words. Galaxies: kinematics and dynamics – Galaxies: elliptical and lenticular, cD – Galaxies: structure – dark matter

1. INTRODUCTION

The problem of dark matter (DM) and its contribution to the total dynamical mass of various types of galaxies remains to be one of the most important unsolved questions of the contemporary astronomy. Although the fact that DM dominates the mass of spiral galaxies is a well established fact (see e.g., Sanders 2010), very recently it was discovered that the rotation curves (which provide the rotation velocity as a function of the disk radius) for the outer disks of six massive star-forming galaxies at redshifts z between approximately 0.6 and 2.6 are not constant, as observed in the local Universe, but decrease with radius (Genzel et al. 2017): this result strongly suggests the lack of DM in spirals beyond the local (low-redshift) Universe. On the other hand, the possible lack of DM in early-type galaxies (ETGs) in the local Universe, ellipticals and lenticulars (S0 galaxies), was detected more than 10 years ago at least in some galaxies (see e.g., Romanowsky et al. 2003, Samurović and Danziger 2005). The observational and theoretical works performed so far suggest that the situation is not simple and possibly there exist two classes of ETGs, one in which the DM content is negligible and the other in which DM dominates the visible, stellar, matter in the outer parts of these galaxies (see e.g. Samurović 2014). We here note that the detection of DM in ETGs is much more complicated than in the case of their spiral counterparts. Namely, ETGs lack cool gas and the usage of 21-cm observations to trace kinematics of neutral hydrogen out to large radii is not feasible in most of the cases. Therefore, other methodologies have to be used in order to measure the total dynamical mass out to large galactocentric radii which is of special importance because DM is expected to dominate luminous matter there. The description of various observational techniques and the theoretical appro-

aches for the study of DM in ETGs are presented e.g. in Samurović (2007) and the update is provided in Samurović (2014, 2016) where we also provided a list of advantages and disadvantages of both methodologies used in the present paper, Newtonian, and MOND (Modified Newtonian Dynamics, Milgrom 1983). Therefore, we refer the interested reader to the aforementioned references and here provide only some most important recent advances.

The advent of the integral field spectroscopy provides a new useful technique of study of ETGs (review in Cappellari 2016) and is related to the study of integrated stellar spectra in a sense that this is an improvement of the long-slit observations used earlier because of the larger spatial coverage. This is important because the only tracer of the gravitational potential which is available for all galaxies is the integrated stellar light. Using the integral field spectroscopy it is now possible to perform measurements of stellar kinematics in ETGs out to $2-3$ effective radii ($R_{\rm e}$) (and even beyond) (e.g. van de Sande et al. 2017).

Globular clusters (GCs) are a very useful tool in the study of DM in ETGs and the reconstruction of the evolutionary history of galaxies in the local Universe. They extend out to several effective radii thus making it possible to study the gravitational potential and the total cumulative mass of the given galaxy out to very distant regions where it is expected that DM dominates the visible matter. Deason et al. (2012) summarized the results found in the literature for 15 elliptical galaxies for observations based on planetary nebulae and GCs. They found that the fraction of DM within $5R_{\rm e}$ increases with mass, in agreement with findings available in the literature, and one of their results was that a Salpeter initial mass function (IMF) is inconsistent with some of the lower mass galaxies. In Samurović (2014) we used a sample of 10 ETGs coming from the SLUGGS (SAGES Legacy Unifying Globulars and Galaxies Survey, where SAGES is the Study of the Astrophysics of Globular Clusters in Extragalactic Systems) sample[1] of Pota et al. (2013) as tracers of the gravitational potential in both the Newtonian (mass-follows-light and DM models) and the MOND approaches and found that the Newtonian mass-follows-light models without a significant amount of DM can provide successful fits for only one galaxy (NGC 2768) whereas the remaining nine ETGs require various amounts of DM in their outer parts (beyond $2-3R_{\rm e}$); in the same paper various MOND models were also studied and it was found that MOND alone is not sufficient to fully explain the dynamics of six galaxies in the sample.

In this paper we will rely on the sample of ETGs with GCs taken from the SLUGGS database. The SLUGGS survey uses the combination of the Subaru/Suprime-Cam wide-field imaging with spectra from the Keck/DEep Imaging Multi-Object Spectrograph (DEIMOS). The results published by the SLUGGS team strongly suggest that the wide-field imaging can give clues about assembly history of the given host galaxy. Also, the combination of the high-velocity resolution data obtained by DEIMOS, provides the opportunity to study the dynamics and the metallicity of the field stars and of the GCs out to several $R_{\rm e}$ thus providing important clues on galaxy dynamics. Very recently, the SLUGGS team has published a catalog of over 4000 GC radial velocities in 27 nearby ETGs (Forbes et al. 2017b) and from it we analyze two lenticular galaxies, NGC 1023 and NGC 4526. Several important results of the SLUGGS analysis include the following findings (Alabi et al. 2017) which are listed here. A high DM fraction and average DM density within 5 $R_{\rm e}$ were found and, more precisely, a DM fraction ranging from 0.1 to 0.9 was measured: this fraction increases with the galaxy stellar mass and is generally independent of the environment of the given galaxy. ETGs with low DM fractions within $5R_{\rm e}$ are those with stellar masses approximately equal to $10^{11}M_{\odot}$ and diffuse DM halos. Also, Alabi et al. (2017) found that S0 and elliptical galaxies are found in DM halos with similar structural properties and assembly epochs. It can be seen from their work that some S0s show a decreasing DM fraction with increasing galaxy stellar mass (in contrast to ellipticals) and Alabi et al. (2017) suggest that this observed difference is due to a "fundamental difference in their dominant late-phase mass assembly channel". In our recent paper (Vudragović et al. 2016), based on the analysis of the sample of 2180 nearby galaxies of all morphological types, we found that there is an indication that ellipticals and lenticulars may share the similar formation scenario based on statistical tests of the distribution of the h_4 parameter which determines the symmetric departures from the Gaussian (equivalent to the s_4 parameter used below). In another recent SLUGGS paper, Forbes et al. (2017a) used 3.6 μm imaging from the Spitzer Space Telescope to decompose the profiles of ETGs in their sample and to also measure the total stellar mass and effective radii in a homogeneous way and we use their results in our analysis below.

In our papers (Samurović 2014, Samurović et al. 2014) based on Pota et al. (2013) we have analyzed 11 SLUGGS galaxies and the two galaxies from the present paper will be placed in the broader cosmological context together with them. The reason why NGC 1023 and NGC 4526 were chosen here lies in the fact that in our previous work (Samurović 2014) only one S0 galaxy was studied and was put into the cosmological context; in that paper we checked whether the features of ETGs agree with the conclusions coming from cosmological simulations. This is important for study of possible different assembly channels. Two S0 galaxies studied in the present paper allowed us to perform the desired analysis since the number of observed GCs was sufficient to calculate the velocity dispersion at seve-

[1] http://sluggs.swin.edu.au

ral galactocentric radii.[2] Also, the number of ETGs and especially S0 galaxies studied using the MOND methodology is still small which means that the analysis of two new objects can provide new insights related to this approach.

The plan of this paper is as follows: in Section 2 we present the basic observational data related to NGC 1023 and NGC 4526 concerning photometry and GCs and the results concerning kinematics. In Section 3 theoretical aspects of the Jeans analysis of dynamics are described and the Jeans equation in both Newtonian and MOND approach is used to determine the best-fit parameters for our dynamical models. In Section 4 we discuss our results and place both studied lenticular galaxies in a broader context and, finally, in Section 5 we present the conclusions.

2. OBSERVATIONAL DATA AND KINEMATICS OF NGC 1023 AND NGC 4526

For the basic observational information regarding two lenticular galaxies, subject of the present work, we rely on the recent papers by Forbes et al. (2017a,b) and Alabi et al. (2017). If some information comes from a different source, the appropriate reference will be quoted. Throughout the paper, the dimensionless Hubble constant $h_0 = 0.70$ is assumed.

2.1. NGC 1023

NGC 1023 is a lenticular galaxy at the distance $D = 11.1$ Mpc which means that $1' \approx 3.23$ kpc and $1'' \approx 53.83$ pc. The effective radius is $R_e = 48$ arcsec and the systemic velocity is $v_{sys} = 602\,\mathrm{km\,s^{-1}}$. The Sérsic index is $n_* = 4.2$ (see below). The absolute B-band magnitude of NGC 1023 is $M_B = -20.61$ and its total apparent corrected B-V color is equal to 0.91 where both values are taken from the HyperLeda database.

2.2. NGC 4526

NGC 4526 is also a lenticular galaxy and is found at the distance $D = 16.4$ Mpc which means that $1' \approx 4.77$ kpc and $1'' \approx 79.54$ pc. The effective radius is $R_e = 32.4$ arcsec and the systemic velocity is $v_{sys} = 617$ km s^{-1}. The Sérsic index is $n_* = 3.6$ (see below). The absolute B-band magnitude of NGC 4526 is $M_B = -20.48$ and its total apparent corrected B-V color is equal to 0.89 where both values are again taken from the HyperLeda database.

As can be seen from the observational data for both lenticulars, they both show similar features. However, as will be shown below, whereas some other features will be very similar, some calculated quantities will be significantly different.

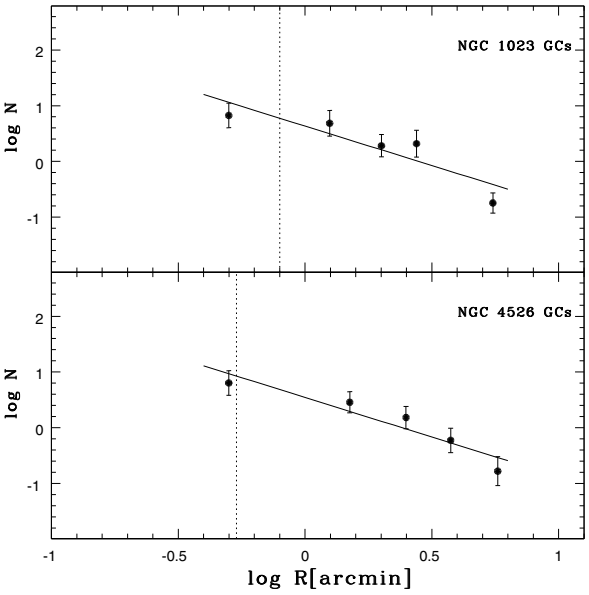

Fig. 1. *Radial distribution of the total sample of GCs of the lenticular galaxies NGC 1023 (upper panel) and NGC 4526 (lower panel). A power law is fitted with solid lines to the radial surface density in both cases: $N \propto R^{-\gamma}$. For NGC 1023, $\gamma = 1.416$ and for NGC 4526, $\gamma = 1.420$. The vertical dotted line, here and in all plots below, represents the value of one effective radius.*

2.3. Globular clusters of NGC 1023 and NGC 4526: determination of kinematics

In the present paper we use two lenticular SLUGGS galaxies coming from the paper by Forbes et al. (2017b): the number of GCs for NGC 1023 and NGC 4526 are 113 and 107, respectively. In both cases we worked with a *total* sample of GCs to have more clusters per bin, i.e., we do not make a distinction between red and blue objects since our goal is to determine as accurately as possible the velocity dispersion and departures from the Gaussian in the distribution of GCs[3]. The amount of rotation found for GCs can be important for establishing the host galaxy merger history and for our sample we used the values $v_{rot} = 119$ km s^{-1} and $v_{rot} = 142$ km s^{-1}, for NGC 1023 and NGC 4526, respectively, based on Alabi et al. (2017). As can be seen, both galaxies show a significant amount of rotation.

From the available data we calculate values of the GC density-profile exponent γ coming from the power-law fits, $N \propto R^{-\gamma}$. We found that $\gamma = 1.416 \pm 0.634$ for NGC 1023 and $\gamma = 1.420 \pm 0.281$ for NGC 4526. Both cases are plotted in Fig. 1. These values will be used below in solving the Jeans equation for both galaxies.

[2]The number of observed GCs in the remaining five lenticulars from the SLUGGS survey (NGC 2974, NGC 3607, NGC 4459, NGC 5866 and NGC 7457) is low and it varies between 20 and 39 and was thus insufficient for the present analysis.

[3]As noted earlier in Samurović (2014), one should bear in mind that red and blue GCs may in principle have different kinematics and their velocity anisotropies may be different.

Also, from the available data we determine the kinematics of both lenticulars, NGC 1023 and NGC 4526, based on their GCs which is given in Table 1 and also in Fig. 2: from the top to the bottom of Fig. 2 we plot as function of radius, the radial velocity, velocity dispersion, s_3 and s_4 parameters which describe skewness and kurtosis, i.e., asymmetric and symmetric departures from the Gaussian, respectively.

The following expressions for calculations of the velocity dispersion, and departures from the Gaussian s_3 and s_4, together with their errors were used (see Joanes and Gill 1998):

$$\sigma = \sqrt{\frac{1}{N-1}\sum_{i=1}^{N}(v_i - v_{\rm sys})^2} \pm \frac{\sigma}{\sqrt{2(N-1)}}, \quad (1)$$

$$s_3 = \frac{N}{(N-1)(N-2)}\sum_{i=1}^{N}\left(\frac{v_i - v_{\rm sys}}{\sigma}\right)^3 \pm \sqrt{\frac{6}{N}}, \quad (2)$$

and

$$s_4 = \frac{N(N+1)}{(N-1)(N-2)(N-3)}\sum_{i=1}^{N}\left(\frac{v_i - v_{\rm sys}}{\sigma}\right)^4 - 3\frac{(N-1)^2}{(N-2)(N-3)} \pm \sqrt{\frac{24}{N}}, \quad (3)$$

where N is the number of GCs in a given bin, v_i is the velocity of the given GC and $v_{\rm sys}$ is the systemic velocity.

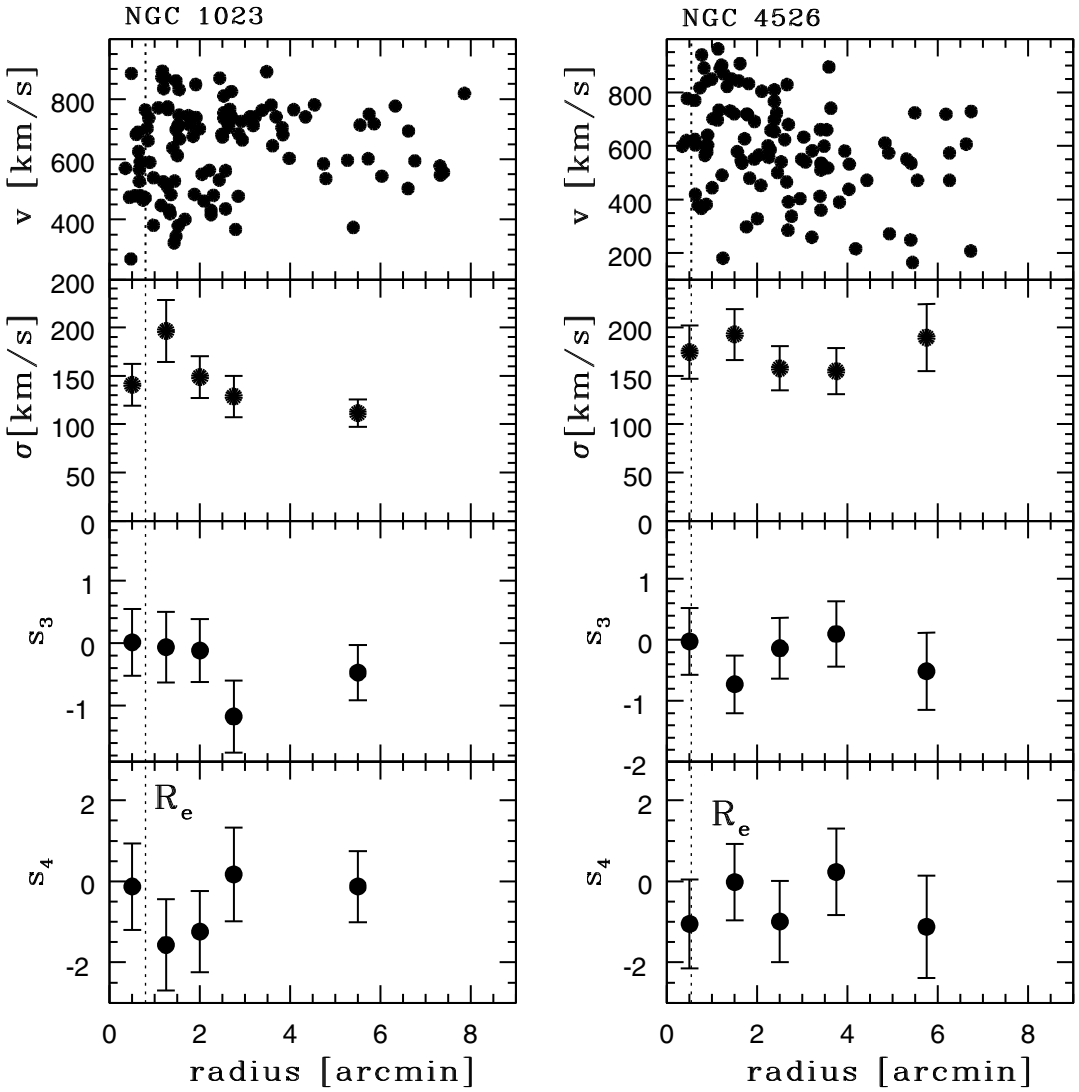

Fig. 2. *Kinematics of GCs belonging to NGC 1023 and NGC 4526. From top to bottom: radial velocities of GCs, velocity dispersions, asymmetric (s_3) and symmetric departures (s_4) from Gaussian as function of radius. See text for details.*

Table 1. Projected velocity dispersion measurements of GCs in NGC 1023 and NGC 4526.

r (arcmin) (1)	σ (km s^{-1}) (2)	err_σ (km s^{-1}) (3)	s_3 (4)	err_s_3 (5)	s_4 (6)	err_s_4 (7)	N (8)
Total sample of GCs of NGC 1023							
0.50	141	22	0.01	0.53	-0.13	1.07	21
1.25	196	33	-0.07	0.56	-1.57	1.12	19
2.00	149	22	-0.12	0.50	-1.24	1.00	24
2.75	129	22	-1.18	0.58	0.17	1.15	18
5.50	111	14	-0.47	0.44	-0.13	0.88	31
Total sample of GCs of NGC 4526							
0.50	175	28	-0.02	0.55	-1.05	1.10	20
1.50	193	27	-0.73	0.47	-0.02	0.94	27
2.50	158	23	-0.14	0.50	-0.99	1.00	24
3.75	155	25	0.10	0.53	0.23	1.07	21
5.75	190	36	-0.51	0.63	-1.12	1.26	15

NOTES – Col. (1): radial bin. Col. (2): velocity dispersion. Col. (3): formal errors for the velocity dispersion. Col. (4): s_3 parameter. Col. (5): formal errors for the s_3 parameter. Col. (6): s_4 parameter. Col. (7): formal errors for the s_4 parameter. Col. (8): number of GCs in a given bin.

The main difference between the two galaxies is the velocity dispersion profile (see Fig. 2): whereas in the outermost bin for NGC 1023 we notice a declining profile with the velocity dispersion equal to 111 km s^{-1}, in the case of NGC 4526 we see that the increase of the velocity dispersion is detected, namely the value of the velocity dispersion reaches 190 km s^{-1}. Also, for NGC 4526, the intermediate points (at 2.50 and 3.75 arcmin) show a constant value of the velocity dispersion (≈ 155 km s^{-1}). As can be seen from Table 1 the last two bins of NGC 4526 contain 36 GCs in total and thus the error bars are larger than in the case of NGC 1023 for which there are 31 GCs in the outermost bin. Thus, as an additional test, for NGC 4526 we placed 36 GCs in one outermost bin centered at 5 arcmin and obtained $\sigma = 168 \pm 20$ km s^{-1}; this means that $v_{\rm rms} = \sqrt{v_{\rm rot}^2 + \sigma^2} = 220$ km s^{-1} and this does not change the results of all our models presented below.

3. THE JEANS MODELLING OF NGC 1023 AND NGC 4526

Our analysis is based on solving of the Jeans equation: in our modeling procedure we follow closely the approach applied earlier in Samurović (2014, 2016) and below several major formulas are given. We use the following spherical Jeans equation which provides connection between the velocity distribution, anisotropy of tracers and the total dynamical mass (e.g., Binney and Tremaine 2008) for both methodologies, Newtonian ("N") and MOND ("M"):

$$\frac{{\rm d}\sigma_r^2}{{\rm d}r} + \sigma_r^2 \frac{(2\beta + \alpha)}{r} = a_{N;M} + \frac{v_{\rm rot}^2}{r}. \qquad (4)$$

Here, $a_{N;M}$ is an acceleration term which is different for each approach: (i) in the Newtonian approach it is equal to $a_N = -\frac{GM(r)}{r^2}$ and (ii) for MOND ('M') models $a_M \mu(a_M/a_0) = a_N$ (below the expressions of the function μ are given). The radial velocity dispersion is designated with σ_r and $\alpha = d\ln\rho/d\ln r$ is the slope of the density of GCs and is taken to be 2.42 for both galaxies, since $\gamma \approx 1.42$, as given above (see Fig. 1). As usual, the rotation and the dispersion profile are folded into a root mean square velocity profile $v_{\rm rms} = \sqrt{v_{\rm rot}^2 + \sigma^2}$.

In all our models we take into account the issue of the anisotropy of the orbits of GCs expressed using the usual form:

$$\beta = 1 - \frac{\overline{v_\theta^2}}{\sigma_r^2}, \qquad (5)$$

where $\overline{v_\theta^2} = \overline{v_\theta}^2 + \sigma_\theta^2$ and $0 < \beta < 1$ means that the orbits are predominantly radial (equivalent to $s_4 > 0$), whereas for $-\infty \leq \beta < 0$ the orbits are mostly tangential (equivalent to $s_4 < 0$) (Gerhard 1993).

The projected line-of-sight velocity dispersion is equal to:

$$\sigma_p^2(R) = \frac{\int_R^{r_{\rm t}} \sigma_r^2(r)\left[1 - (R/r)^2\beta\right]\rho(r)(r^2 - R^2)^{-1/2} r dr}{\int_R^{r_t} \rho(r)(r^2 - R^2)^{-1/2} r dr}, \qquad (6)$$

where $r_{\rm t}$ is the truncation radius and it extends beyond the observed kinematical point of the highest galactocentric radius (Binney and Mamon 1982).

In all our dynamical models, we deal with three cases of anisotropies:

a) the isotropic case for which $\beta = 0.00$,

b) the theoretically based case (Mamon and Łokas 2005), for which:

$$\beta(r) = \beta_0 \frac{r}{(r + r_a)}, \quad (7)$$

where $\beta_0 \simeq 0.5$ and $r_a \simeq 1.4 R_{\rm e}$. This is radially dominated since $\beta > 0$ comes from theoretical expectations from merging collisionless systems; we denote the values of the β parameter thus calculated as $\beta_{\rm lit}$ in the text below, and

c) mildly tangentially dominated case, for which we have a hint from the negative values of the s_4 parameter for the majority of calculated points of both lenticulars (see Fig. 2, lowest panel), for which $\beta = -0.20$ is assumed.

Our best-fitting results obtained using the Jeans equation are shown in Figs. 3–7 below.

In both approaches we always rely on a Newtonian constant mass-to-light ratio Sérsic model (see Samurović 2014) that uses field stars of both lenticulars and for which the Sérsic indices $n_* = 4.2$ and $n_* = 3.6$ for NGC 1023 and NGC 4526, respectively, were used. Here, the stellar mass-to-light is a free parameter (see Romanowsky et al. 2009) and the equation which provides the circular velocity reads:

$$\begin{aligned} v_{\rm c}^2(r) &\equiv \frac{GM(r)}{r} \\ &= \frac{G(M/L_*)L_*}{r} \times \\ &\left\{1 - \frac{\Gamma\left[(3-p)n_*, (r/a_s^*)^{1/n_*}\right]}{\Gamma\left[(3-p)n_*\right]}\right\}, \quad (8) \end{aligned}$$

where n_* and a_s^* are the Sérsic index and scale radius for the stellar component respectively, and p is a function of n_*. For further details the reader is referred to Samurović (2014).

In the case of the usage of the Navarro-Frenk-White (NFW, Navarro, Frenk and White 1997) formula, to this visible mass we add the dark component (see below).

When we compare our estimates of the dynamically inferred values of the mass-to-light ratio in various models to the predictions coming from several stellar population synthesis (SPS) models we rely on the paper by Bell and De Jong (2001). The models, together with metallicity and IMFs used are given in Table 2. The models are based on the corrected $B - V$ color from the HyperLeda database for both lenticular galaxies. The values found in Table 2 are compared with the dynamically established values of the mass-to-light ratios in order to infer the contribution of the DM component. The chosen value of the metallicity was based on the work of Casuso et al. (1996) who used the Lick index ($\rm Mg_2$) as an indicator of metallicity. Both of our galaxies have the value of the $\rm Mg_2$ index equal to approximately 0.30: from the HyperLeda database we find that for NGC 1023 the value of this index is 0.293 and for the galaxy NGC 4526 the value is 0.268. Therefore, from Fig. 3 of Casuso et al. (1996), one can conclude that the value $Z = 0.02$ for which we determine the values of the stellar mass-to-light ratios, is an accurate approximation. In Table 2 we present estimates of the mass-to-light ratios used assuming that there are no color gradients, i.e., that the colors are constant throughout both galaxies. This is indeed true for NGC 4526 for which there is a negligible decrease in the value of the $B - V$ color (see Poulain and Nieto 1990). However, for NGC 1023 there is a gradual decrease, namely at 180 arcsec $B - V$ drops to ≈ 0.4 (Debattista et al. 2002). This means that the SPS models then predict *lower* estimates of the mass-to-light ratio, $M/L_{\rm B} \sim 1$. Therefore, our estimates for NGC 1023 based on the various SPS models should be considered as the *upper limits* for the stellar mass-to-light ratios. The age gradients found in Kuntschner et al. (2010) suggest that for NGC 1023 the age is constant whereas for NGC 4526 there is a mild increase in the age from the center (but within the error bars consistent with constant age) and we thus consider that the age gradients do not play an important role in our estimates.

Table 2. Values of the predicted stellar mass-to-blue-light ratios in various theoretical SPS models for both lenticular galaxies.

Name		BC model	PEGASE model	IP13 model1	IP13 model2	IP13 model
	IMF	Salpeter	Salpeter	Kroupa	Kroupa	Salpeter
	metallicity (Z)	0.02	0.02	≤ 0.03	≤ 0.03	≤ 0.03
(1)		(2)	(3)	(4)	(5)	(6)
NGC 1023	M/L_*^B	6.45	7.07	4.20	4.75	8.16
NGC 4526	M/L_*^B	6.03	6.61	3.85	4.33	7.43

NOTES – The theoretical predictions of stellar mass-to-light ratios are given in the B-band. Col. (1): Name of the galaxy. Col. (2): SPS Bruzual and Charlot (Bruzual and Charlot 2003, BC) model with Salpeter IMF for $Z = 0.02$. Col. (3): SPS PEGASE (Fioc and Rocca-Volmerange 1997) model with Salpeter IMF for $Z = 0.02$. Col. (4): the exponential SFH model with the Kroupa (1998) IMF (Into and Portinari 2013, IP13). Col. (5): the disc galaxy model based on the Kroupa (1998) IMF (Into and Portinari 2013, IP13). Col. (6): the disc galaxy model based on the Salpeter IMF (Into and Portinari 2013, IP13).

For each our Jeans model we calculate the χ^2 statistic:

$$\chi^2 = \sum_{i=1}^{N} \left[\frac{p_i^{\rm obs} - p_i^{\rm mod}}{\Delta p_i^{\rm obs}} \right]^2 , \qquad (9)$$

where N is the number of data points, $p_i^{\rm obs}$ are the observed data points, the model values are given with $p_i^{\rm mod}$, and $\Delta p_i^{\rm obs}$ are the uncertainties on the observed values at the given radius. The reduced $\bar{\chi}^2$ values will be given for each best-fitting model.

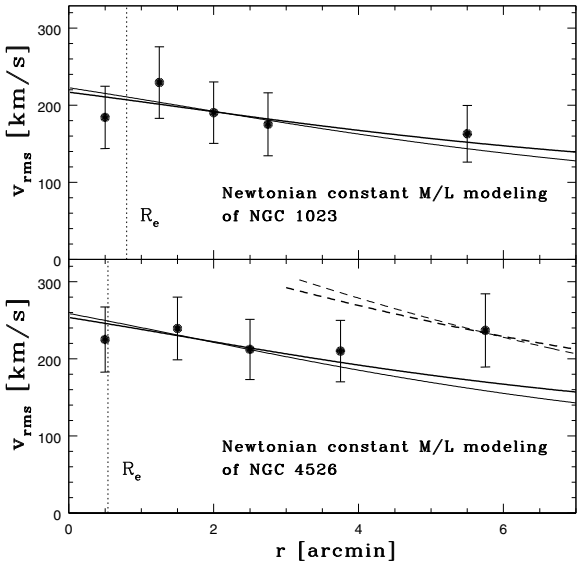

Fig. 3. *Jeans modeling of the GCs of NGC 1023 (upper panel) and NGC 4526 (lower panel) for the Newtonian mass-follows-light cases. The thick solid lines for both galaxies are used for the isotropic case ($\beta = 0.00$) and the thin solid lines for both galaxies are used for the radially anisotropic theoretical case ($\beta = \beta_{\rm lit}$), see the text for details). The values of the mass-to-light ratios ($M/L_{\rm B}$) for NGC 1023 are 5.4 and 7.0 for the isotropic and radially anisotropic case, respectively. For NGC 4526, the values of the mass-to-light ratios ($M/L_{\rm B}$) for NGC 4526 are 9.8 and 13.0, for the isotropic and radially anisotropic case, respectively, where only four inner points were fitted. For NGC 4526 two additional fits, shown with dashed lines, were made for the outermost point: the values of the mass-to-light ratios are: 22.1 and 33.2 for the isotropic (thick line) and radially anisotropic case (thin line), respectively.*

The results shown in Fig. 3 are obtained using the purely constant mass-to-light ratio model for both lenticulars. One can see in the upper panel that NGC 1023 can be successfully modeled with the stellar component alone: for the isotropic case the best-fitting model is $M/L_{\rm B} = 5.4$ (with $\bar{\chi}^2 = 0.24$) and for the radially anisotropic theoretical case ($\beta = \beta_{\rm lit}$) the best-fitting model is $M/L_{\rm B} = 7.0$ (with $\bar{\chi}^2 = 0.30$). Note that in this Figure, and also in all other models below, the best tangentially anisotropic fit ($\beta = -0.20$) was not plotted because it practically coincides with the isotropic case albeit with the smaller mass-to-light ratio: for NGC 1023 the best-fitting value for the tangentially anisotropic fit is $M/L_{\rm B} = 4.6$ (with $\bar{\chi}^2 = 0.21$). Thus one can conclude that for NGC 1023 DM is not needed, if one assumes the Salpeter IMF (see Table 2) or at least it does not dominate the visible stellar matter: from Table 2 one can see that the theoretical predictions based on the SPS models suggest that the mass-to-light ratio in the B-band varies between 4.20 (for the Kroupa IMF) and 8.16 (for the Salpeter IMF).

The case of the lenticular galaxy NGC 4526 shown in the lower panel of Fig. 3 is more complex. The two solid lines are best fits obtained when *only the four inner points* are fitted. The obtained values are high: $M/L_{\rm B} = 9.8$ (with $\bar{\chi}^2 = 0.14$) for the isotropic case and $M/L_{\rm B} = 13.0$ (with $\bar{\chi}^2 = 0.22$) for the radially anisotropic case (the tangentially best-fitting anisotropic case for inner four points with $M/L_{\rm B} = 7.6$, with $\bar{\chi}^2 = 0.13$, is not shown). The obtained values provide a hint of a certain amount of DM even in the inner parts of this galaxy. In Fig. 3 we also fitted the outermost point at 5.75 with two constant mass-to-light models: the values are high, $M/L_{\rm B} = 22.1$ for the isotropic case and $M/L_{\rm B} = 33.2$ for the radially anisotropic case. Such high values imply a significant amount of DM in outer regions of NGC 4526 which means that the dark component dominates there and the fraction of DM is at ranges form at least 0.66 (for the isotropic case) to 0.78 (for the radially anisotropic case) in these outer parts.

3.1. Newtonian DM models

Since the constant mass-follows-light model cannot reproduce the dynamics of NGC 4526 (and also due to the fact that, if the Kroupa IMF is assumed in the case of NGC 1023, DM is needed) we here apply Newtonian approach with an additional dark component in a form of the NFW DM halo. The enclosed mass of such a halo is:

$$M(x) = 4\pi\rho_{\rm s} r_{\rm s}^3 \left[\ln(1+x) - \frac{x}{1+x} \right], \qquad (10)$$

where $x = r/r_{\rm s}$, $r_{\rm s}$ is the scale radius at which the logarithmic slope of the NFW density profile is -2, while $\rho_{\rm s}$ is the density at that radius. Thus determined halo is added to the visible, stellar mass calculated using the Sérsic model given above. Therefore, for each NFW DM model we have three free parameters: the stellar mass-to-light ratio $(M/L_{\rm B})_*$, scale radius $r_{\rm s}$, and density $\rho_{\rm s}$. Also, for our NFW models we calculate the concentration parameter ($c_{\rm vir} \equiv r_{\rm vir}/r_{\rm s}$) and the virial mass $M_{\rm vir} \equiv 4\pi\Delta_{\rm vir}\rho_{\rm crit} r_{\rm vir}^3/3$ where the critical density is $\rho_{\rm crit} = 1.37 \times 10^{-7} M_\odot {\rm pc}^{-3}$ and the critical overdensity is $\Delta_{\rm vir} = 101$.

In Fig. 4 we present our best-fitting results for the NFW DM models for the tested anisotropies.

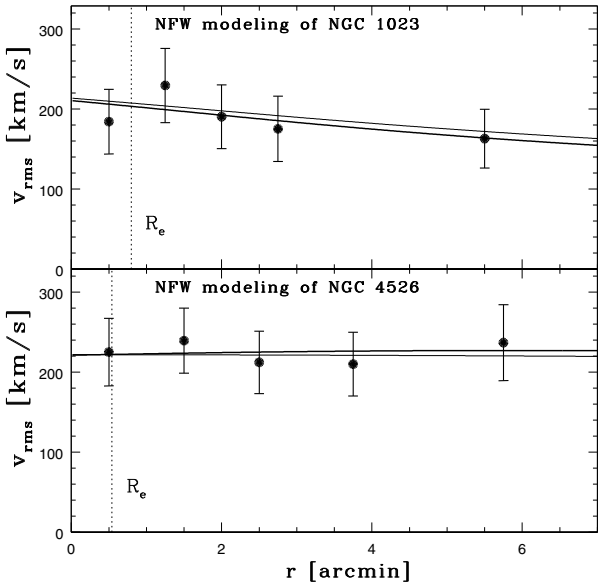

Fig. 4. *The NFW modeling of GCs of NGC 1023 and NGC 4526. In the case of NGC 1023 (upper panel), the thick solid line is for the isotropic case ($\beta = 0.00$) for which the mass-to-light of the stellar component in the B-band is $M/L_* = 5.5$ and $r_s = 400$ arcsec and $\rho_s = 0.0150 M_\odot \mathrm{pc}^{-3}$, and the thin solid line is for the radially anisotropic theoretical case ($\beta = \beta_{\mathrm{lit}}$), for which $M/L_* = 5.5$ and $r_s = 200$ arcsec and $\rho_s = 0.0200 M_\odot \mathrm{pc}^{-3}$. In the case of NGC 4526 (lower panel), the thick solid line is for the isotropic case ($\beta = 0.00$) with $M/L_* = 5.0$ and $r_s = 600$ arcsec and $\rho_s = 0.0090 M_\odot \mathrm{pc}^{-3}$, and the thin line is for the radially anisotropic theoretical case ($\beta = \beta_{\mathrm{lit}}$), for which $M/L_* = 7.0$ and $r_s = 800$ arcsec and $\rho_s = 0.070 M_\odot \mathrm{pc}^{-3}$.*

For NGC 1023 (upper panel of Fig. 4) we find that the best-fitting values for the isotropic case are $M/L_* = 5.5$, $r_s = 400$ arcsec, and $\rho_s = 0.0150 M_\odot \mathrm{pc}^{-3}$ with $\bar{\chi}^2 = 0.20$, whereas the best-fitting model for the radially anisotropic theoretical case is described with $M/L_* = 5.5$, $r_s = 200$ arcsec, and $\rho_s = 0.0200 M_\odot \mathrm{pc}^{-3}$ with $\bar{\chi}^2 = 0.23$. The best-fitting values for the tangentially anisotropic case (not shown) were $M/L_* = 6.0$, $r_s = 200$ arcsec, and $\rho_s = 0.0300 M_\odot \mathrm{pc}^{-3}$ with $\bar{\chi}^2 = 0.19$.

For the other galaxy NGC 4526 (lower panel of Fig. 4) we find that the best-fitting values for the isotropic case are $M/L_* = 5.0$, $r_s = 600$ arcsec, and $\rho_s = 0.0090 M_\odot \mathrm{pc}^{-3}$ with $\bar{\chi}^2 = 0.12$, whereas the best-fitting values for the radially anisotropic theoretical case are $M/L_* = 7.0$, $r_s = 800$ arcsec, and $\rho_s = 0.0070 M_\odot \mathrm{pc}^{-3}$ with $\bar{\chi}^2 = 0.11$. The best-fitting values for the tangentially anisotropic case (not shown) were $M/L_* = 8.0$, $r_s = 700$ arcsec, and $\rho_s = 0.0090 M_\odot \mathrm{pc}^{-3}$ with $\bar{\chi}^2 = 0.19$.

Taking into account the uncertainties related to anisotropy, we calculated the following values of the concentration parameter of the NFW halo and the virial mass for both galaxies: $c_{\mathrm{vir}} = 10.89^{+2.12}_{-2.54}$ for NGC 1023, $c_{\mathrm{vir}} = 7.81^{+2.87}_{-1.83}$ for NGC 4526, and $M_{\mathrm{vir}} = 7.47^{+5.23}_{-4.10} \times 10^{11} M_\odot$ for NGC 1023, $M_{\mathrm{vir}} = 3.00^{+4.62}_{-1.65} \times 10^{12} M_\odot$ for NGC 4526.

3.2. MOND models

As in our previous works (Samurović 2014, Samurović et al. 2014, Samurović 2016) we tested three MOND models based on three different interpolating formulas using the Jeans equation in the spherical approximation. We relied on the methodology described in detail in Samurović (2014) and we here provide some necessary basic information. In all tested MOND models there is *only one* free parameter, i.e. the total stellar mass-to-light ratio, which is based on the visible stellar mass only: by varying the value of the mass-to-light ratio which best describes the observed velocity dispersions three different figures are obtained and are shown below – the plotted curves represent the best-fitting cases.

The Newtonian acceleration is given as $a_{\mathrm{N}} = a\mu(a/a_0)$, where a is the MOND acceleration. The value of the universal constant is $a_0 = 1.35^{+0.28}_{-0.42} \times 10^{-8}$ cm s^{-2}, (Famaey et al. 2007) and $\mu(x)$ is the MOND interpolating function which is different for each MOND model.

A simple MOND formula (Famaey and Binney 2005) is given by:

$$\mu(x) = \frac{x}{1+x}\,, \tag{11}$$

where $x = a/a_0$ here and below.

The standard MOND formula (Sanders and McGaugh 2002) is given by:

$$\mu(x) = \frac{x}{\sqrt{1+x^2}}. \tag{12}$$

The toy MOND model (Bekenstein 2004) is described with:

$$\mu(x) = \frac{-1+\sqrt{1+4x}}{1+\sqrt{1+4x}}. \tag{13}$$

We refer the reader to Samurović and Ćirković (2008) where the expressions for the circular velocities for all three functions were given.

The best-fitting models for all three tested MOND models are presented in Figs. 5-7.

The simple MOND model provides successful fits for NGC 1023 (upper panel of Fig. 5) for all tested cases and the values for the stellar mass-to-light ratio are: 3.4 for the isotropic model and 4.8 for the radially anisotropic model with $\bar{\chi}^2 = 0.24$ and $\bar{\chi}^2 = 0.20$, respectively. The best-fitting tangentially anisotropic case is not shown, but the best-fitting value is $(M/L_{\mathrm{B}})_* = 2.6$ with $\bar{\chi}^2 = 0.27$. One can conclude that DM is not required in this case.

On the other hand, the case of NGC 4526 (lower panel of Fig. 5) is more complex. The value of the mass-to-light ratio obtained for the isotropic case using the simple MOND formula ($(M/L_{\mathrm{B}})_* = 7.6$

with $\bar{\chi}^2 = 0.18$) and for the tangentially anisotropic case ($(M/L_{\rm B})_* = 5.7$, $\bar{\chi}^2 = 0.15$, not shown) means that the inferred value of the mass-to-light is in agreement with the SPS models from Table 2 and that DM is not needed. However, the case of the radially anisotropic model suggests (the best-fitting value is $(M/L_{\rm B})_* = 10.8$ with $\bar{\chi}^2 = 0.30$) that at least some amount of DM (~ 30 per cent of the total dynamical mass) is necessary to successfully model this lenticular galaxy.

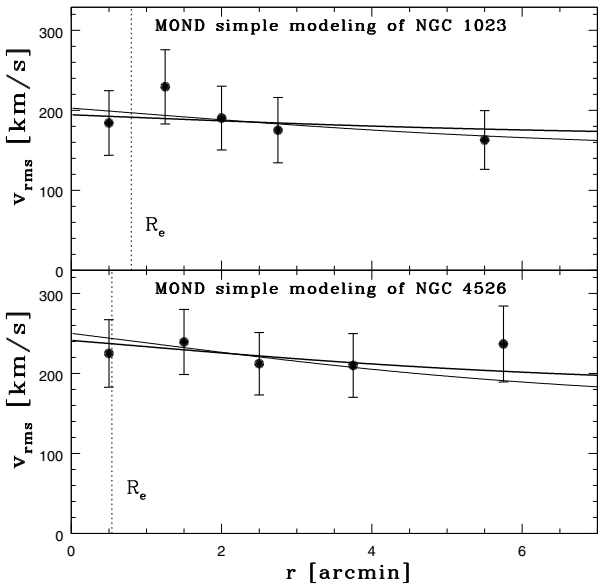

Fig. 5. *The MOND modeling of GCs of NGC 1023 (upper panel) and NGC 4526 (lower panel) for the simple formula. The values of the mass-to-light ratio in the B-band of the stellar component for each case are: 3.4 and 4.8 for the isotropic and radially anisotropic theoretical case, respectively (for NGC 1023, upper panel) and 7.6 and 10.8 for the isotropic and radially anisotropic theoretical case, respectively (for NGC 4526, lower panel).*

The standard MOND model also provides successful fits for NGC 1023 (upper panel of Fig. 6) for all tested cases and the values for the stellar mass-to-light ratio are again consistent with a no dark-matter hypothesis: 4.2 for the isotropic model (with $\bar{\chi}^2 = 0.23$) and 5.8 for the radially anisotropic model (with $\bar{\chi}^2 = 0.19$). The best-fitting tangentially anisotropic case is not shown but the best-fitting value is $(M/L_{\rm B})_* = 3.2$ with $\bar{\chi}^2 = 0.25$. One can conclude that DM is not required in this case.

Once again, the case of NGC 4526 (lower panel of Fig. 6) is more complex. Both values of the mass-to-light ratio obtained for the isotropic case for the standard MOND formula ($(M/L_{\rm B})_* = 9.0$ with $\bar{\chi}^2 = 0.22$) and for the radially anisotropic case ($(M/L_{\rm B})_* = 12.6$, $\bar{\chi}^2 = 0.38$) suggest that DM is needed. For the tangentially anisotropic model ($(M/L_{\rm B})_* = 6.8$, with $\bar{\chi}^2 = 0.18$) DM is, on the other hand, not needed, assuming the Salpeter IMF.

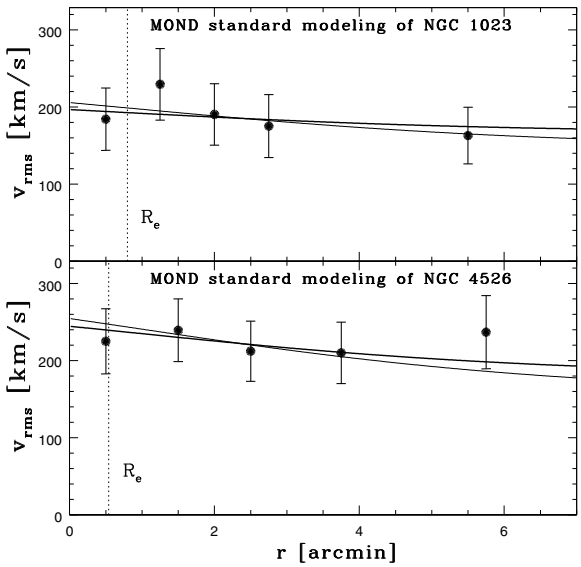

Fig. 6. *The MOND modeling of GCs of NGC 1023 (upper panel) and NGC 4526 (lower panel) for the standard formula. The values of the mass-to-light ratio of the stellar component in the B-band for each case are: 4.2 and 5.8 for isotropic and radially anisotropic theoretical case, respectively (for NGC 1023, upper panel) and 9.0 and 12.6 for isotropic and radially anisotropic theoretical case, respectively (for NGC 4526, lower panel).*

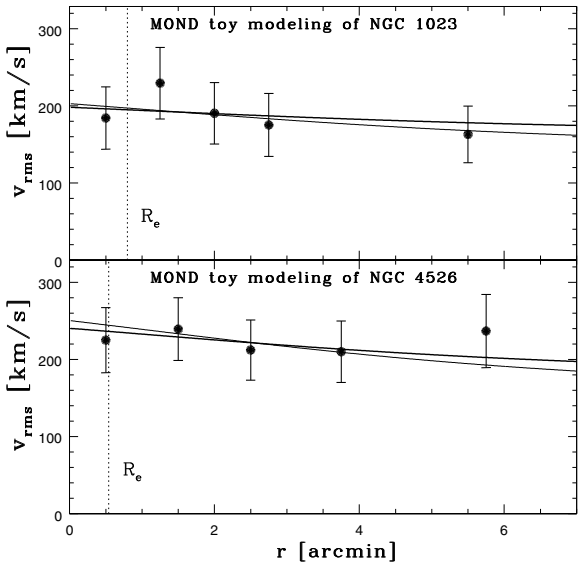

Fig. 7. *The MOND modeling of GCs of NGC 1023 (upper panel) and NGC 4526 (lower panel) for the toy formula. The values of the mass-to-light ratio of the stellar component in the B-band for each case are: 2.8 and 3.8 for isotropic and radially anisotropic theoretical case, respectively (for NGC 1023, upper panel) and 6.0 and 8.8 for isotropic and radially anisotropic theoretical case, respectively (for NGC 4526, lower panel).*

Finally, the toy MOND model once again provides successful fits for NGC 1023 (upper panel of Fig. 7) for all tested cases: the best-fitting value for the isotropic model is $(M/L_{\rm B})_* = 2.8$ with $\bar{\chi}^2 = 0.24$, and for the radially anisotropic model $(M/L_{\rm B})_* = 3.8$ with $\bar{\chi}^2 = 0.20$. The best-fitting value obtained for the tangentially anisotropic model, $(M/L_{\rm B})_* = 2.0$ with $\bar{\chi}^2 = 0.26$, is below the lowest allowed value based on the SPS model as given in Table 2, as is also the case for the isotropic model and the radially anisotropic model is very close to that lowest value $(M/L_{\rm B})_* = 3.85$.

4. DISCUSSION

As can be seen from our results above, although the two lenticulars, NGC 1023 and NGC 4526, share certain similarities (such as B-magnitude, photometric profiles, values of the $\rm Mg_2$ Lick index and the radial distribution of GCs) their mass content is different. Most importantly, their velocity dispersion profiles differ, thus leading to different Jeans models in both methodologies, Newtonian and MOND. For both galaxies we can, however, confirm our previous findings that inside $\sim 3R_{\rm e}$ there is no need for DM, or at least, DM is not dominant form of matter, which is in agreement with what was found for NGC 4472 (Samurović 2012), NGC 1407 and NGC 5846 (Samurović 2014), and NGC 5128 (Samurović 2016), to list just several examples. Beyond $\sim 3R_{\rm e}$ DM becomes more important but its contribution may vary. For example, for the first galaxy of the present study, NGC 1023, the outermost point at $6.9R_{\rm e}$ can be fitted (although not perfectly, see Fig. 3, upper panel) without DM for all cases of anisotropy, if one assumes the Salpeter IMF. If we want to fit exactly that outermost point we need $M/L_{\rm B} = 6.5$ (for the isotropic case) and $M/L_{\rm B} = 9.6$ (for the radially anisotropic case). The latter value, related to the theoretical based radially anisotropic case, suggests the existence of DM, i.e., the DM fraction varies between 0.15 (for the IP13 model based on the Salpeter IMF) and 0.56 (for the IP13 model based on the Kroupa IMF). Because of the gradient in color of this galaxy, the values of DM fraction should be understood as *lower* limits. Our values calculated at $\sim 7R_{\rm e}$ are consistent with the estimate calculated in Alabi et al. (2017) who found that the fraction of DM inside $5R_{\rm e}$ is 0.46 ± 0.13 (for $\beta = -0.5$). For the other lenticular galaxy, NGC 4526, the situation is as follows: for fitting of the outermost point at $10.6R_{\rm e}$ one needs $22.1 \lesssim M/L_{\rm B} \lesssim 33.2$ (see Fig. 3, lower panel) which implies that the contribution of DM in these outermost regions ranges at least between 0.66 (for the IP13 model based on the Salpeter IMF) and 0.78 (again for the IP13 model based on the Salpeter IMF) which is in agreement with the estimate of Alabi et al. (2017) who found the DM fraction equal to 0.75 ± 0.06 (inside $16.75R_{\rm e}$ for $\beta = -0.5$). Our estimates for the outermost point of NGC 4526 based on the IP13 Kroupa IMF provide the following range: 0.83 < DM fraction < 0.88. Both estimates of Alabi et al. (2017) were based on a technique different from that used in our analysis, i.e., they relied on the tracer mass estimator technique.

When we compare the Jeans MOND models of both galaxies we can see that for NGC 1023 all tested MOND formulas provide satisfactory fits to the velocity dispersion without the need for DM whereas all three tested MOND models in the case of NGC 4526 suggest the need of a certain amount of the dark component (the DM fraction of ~ 0.40 for the standard MOND model and ~ 0.15 for the toy MOND model). What is the reason for this difference? In Samurović (2014) we speculated that the "dynamical mass" $M_{\rm dyn} \simeq 1.58 \times 10^{11} M_\odot$ separates two-classes of ETGs: only the galaxies with the mass below this limit can be fitted with MOND without additional DM. The "dynamical mass" for each galaxy can be calculated using the following expression (Bertin et al. 2002):

$$M_{\rm dyn} = K_v \frac{\sigma_0^2 R_e}{G}, \tag{14}$$

where $K_v = 5$ (Cappellari et al. 2006) and σ_0 is the central velocity dispersion taken from Alabi et al. (2017)[4]. For NGC 1023, $\sigma_0 = 183$ km s^{-1}, and for NGC 4526, $\sigma_0 = 233$ km s^{-1}. Thus, we obtain the following values: $M_{\rm dyn} = 1.01 \times 10^{11} M_\odot$ (for NGC 1023) and $M_{\rm dyn} = 1.63 \times 10^{11} M_\odot$ (for NGC 4526). As can be seen, these results are in agreement with our previous findings: NGC 1023 can be modeled without DM using MOND, whereas NGC 4526 for which the "dynamical mass" is just above the established limit cannot be fitted using this methodology without invoking DM. This result confirms a possible existence of breakdown of MOND discussed in Samurović (2014).

Another clue about the differences between the two lenticulars studied in this paper comes from their calculated stellar mass (see Alabi et al. 2017, their Table 1): the stellar mass of NGC 1023 is $M_* = 9.77 \times 10^{10} M_\odot$ and the stellar mass of NGC 4526 is $M_* = 1.82 \times 10^{11} M_\odot$. The difference of the factor of two in estimates of stellar masses of the two galaxies comes from the way they were computed: these etimates were obtained using the K-band data from Alabi et al. (2016) in their Table 2, i.e. $M_K = -24.16$ (NGC 1023) and $M_K = -24.81$ (NGC 4526) assuming $M/L_K = 1.0$ in *both* cases. When we check stellar masses of ETGs belonging to the SLUGGS sample studied in Samurović (2014) we see that *none* of ETGs with stellar masses above $M_* = 1.78 \times 10^{11} M_\odot$ can be fitted in MOND without additional DM (the galaxies for which DM is needed are: NGC 1407, NGC 4278, NGC 4365, NGC 4486 and NGC 5846). The case of the lenticular galaxy NGC 4526 fits into

[4] As noted in Samurović (2014), this expression is only correct for estimating the mass within half-light radius.

this pattern. On the other hand, for stellar mass below $M_* = 1.78 \times 10^{11} M_\odot$ a certain ETG may or may not be fitted in MOND without additional DM (for example, NGC 1400, NGC 2768, NGC 3377 and NGC 4494 can be fitted, but NGC 3115 cannot be fitted without the dark component). Since the lenticular NGC 1023 can be fitted in MOND without DM, it obviously also follows the aforementioned pattern.

We now want to position both lenticulars studied in this paper within the context of other ETGs coming from the SLUGGS sample and studied by us (Samurović 2014) and the results of numerical simulations. Fig. 8 shows the dependence of the concentration parameter as a function of the virial mass.

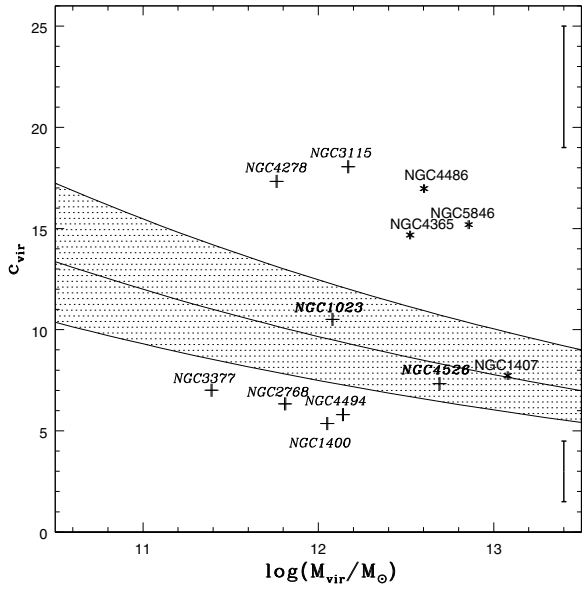

Fig. 8. *The concentration parameter as a function of the virial mass (expressed in solar units). Two lenticulars, NGC 1023 and NGC 4526, the subject of the present paper, are plotted using bold type characters, whereas other galaxies from Samurović (2014) are plotted using regular type characters: the names of the slow (fast) rotators are plotted using Roman characters, with "∗" sign (italics, with "+" sign). The central line of the hatched region is given by Eq. 15, and its limits are determined with 1σ scatter. The vertical solid lines on the right hand side of the plot represent typical error bars for the concentration parameter for two classes of galaxies: the lower line is for the objects below the hatched region, and the upper line is for the objects inside and above the hatched region.*

The hatched area represents the region determined by the mean relation expected from the ΛCDM (cold dark matter plus cosmological constant) model for which the central line is given with:

$$c_{\rm vir}(M_{\rm vir}) \simeq 12 \left(\frac{M_{\rm vir}}{10^{11} M_\odot} \right)^{-0.094}, \qquad (15)$$

and the limits are determined with 1σ scatter (equal to 0.11 dex, see for example, Napolitano et al. 2011). As in Samurović (2014, see Fig. 24), the ETGs are divided into two classes, slow and fast rotators. Both of the lenticular galaxies studied in this paper are fast rotators (see Arnold et al. 2014) as is the galaxy NGC 3115 the only remaining S0 galaxy from the sample studied in Samurović (2014). It is interesting to conclude that both lenticulars studied here fall into the hatched region which means that their concentration parameters agree with the predictions from the numerical simulations, together with the galaxy NGC 1407, the only object belonging to this region from the sample of 10 previously studied ETGs. Here, for the first time, we find that two fast rotators can be described using the results of numerical simulations. It will be interesting to place new ETGs and, especially, new fast rotators, on the $c_{\rm vir} - M_{\rm vir}$ plot as new data (from SLUGGS and other surveys) become available.

5. CONCLUSIONS

In this paper we studied two lenticulars galaxies, NGC 1023 and NGC 4526, which possess GCs that were used to calculate their kinematical parameters. Both galaxies show similar features such as magnitude, photometric profiles, values of the Mg_2 Lick index and the radial distribution of GCs. Using the recently published data from the SLUGGS database we calculated velocity dispersions, as well as departures from the Gaussian function, i.e., the skewness (s_3) and kurtosis (s_4) parameters using standard statistical procedures. We then used the Jeans equation to make dynamical models of both galaxies to infer the DM content in them using the Newtonian approach. We also solved the Jeans equation for three MOND models (based on simple, standard and toy MOND formulas). In solving the Jeans equation in both methodologies, Newtonian and MOND, we allowed several possibilities for anisotropies of orbits: isotropic orbits, tangentially dominated orbits and radially dominated orbits.

Our conclusions are as follows.

(1) The departures from the Gaussian which we estimated from the radial velocities of the sample of GCs of both lenticulars are not large and in most of the bins are consistent with isotropic distribution. Whereas the velocity dispersion of NGC 1023 shows the declining trend, and the value of the velocity dispersion at the outermost point at $\sim 6.9 R_{\rm e}$ is 111 km s^{-1}, for the other galaxy, NGC 4526, the velocity dispersion does not show the declining trend and its value at the outermost point at $\sim 10.6 R_{\rm e}$ reaches 190 km s^{-1} which implies a higher total mass there.

(2) We showed that Newtonian mass-follows-light can provide successful fits for both lenticular galaxies, NGC 1023 and NGC 4526, in the interior up to $\sim 3 R_{\rm e}$, thus confirming our earlier findings, although in the case of NGC 4526 some DM is needed. Beyond $\sim 3 R_{\rm e}$ in the case of NGC 1023, the outermost point at $6.9 R_{\rm e}$ can be fitted without

DM for all cases of anisotropy, if one assumes the Salpeter IMF. If one wants to fit exactly the outermost point one would need $M/L_{\rm B} = 6.5$ (for the isotropic case) and $M/L_{\rm B} = 9.6$ (for the radially anisotropic case): this means that the DM fraction varies between 0.15 (for the IP13 model based on the Salpeter IMF) and 0.56 (for the IP13 model based on the Kroupa IMF). Because of the noted gradient in the $B-V$ color of this galaxy these estimates are the *lower* values. In the case of NGC 4526 a significant amount of DM is needed to fit the outermost point, since $22.1 \lesssim M/L_{\rm B} \lesssim 33.2$ (for isotropic and radially anisotropic cases) and this implies that the contribution of DM in these outermost regions ranges at least between 0.66 (for the IP13 model based on the Salpeter IMF) and 0.78 (again for the IP13 model based on the Salpeter IMF).

(3) We also used the Jeans equation to model both lenticulars by adding the dark halo in the NFW form and placed both galaxies, NGC 1023 and NGC 4526, on the $M_{\rm vir} - c_{\rm vir}$ plot together with other SLUGGS ETGs that we previously analyzed. We find that both galaxies, NGC 1023 and NGC 4526, can be described by the relation expected from the ΛCDM cosmological model. In fact, together with NGC 1407, these are the only 3 galaxies (out of 13 studied SLUGGS objects) that follow this relation. For the first time, we placed two fast rotators on the $M_{\rm vir}-c_{\rm vir}$ plot in the region suggested by numerical simulations. Future studies will certainly provide new insights into positions of more lenticular galaxies in this plot.

(4) We tested three MOND models based on three MOND formulas (standard, simple and toy). In the case of NGC 1023 all three MOND models can fit successfully the observed velocity dispersion without invoking DM since the established mass-to-light ratio in the B-band varies between ~ 3 and ~ 6 which is in agreement with the several tested SPS models (the lower limit calculated for the toy model is below the lowest value allowed by the SPS models). For NGC 4526, all three tested MOND models suggest that there is a need of a certain amount of the dark component with the DM fraction of ~ 0.40 for the standard MOND model and ~ 0.15 for the toy MOND model.

(5) Although both studied lenticulars share some features, their velocity dispersion profiles differ and their mass content is different. We suggest that this difference is due to the difference in their stellar mass: the more massive lenticular galaxy NGC 4526 has also more massive stellar and dark component than the less massive lenticular NGC 1023. The new observations which will include more ETGs of all types, together with improved dynamical models, will certainly clarify this issue.

Acknowledgements – This work was supported by the Ministry of Education, Science and Technological Development of the Republic of Serbia through the project no. 176021, "Visible and Invisible Matter in Nearby Galaxies: Theory and Observations". We acknowledge the usage of the HyperLeda database (http://leda.univ-lyon1.fr). The author acknowledges numerous useful discussions with Dr. Michal Bílek. The author expresses his gratitude to the referee for numerous useful suggestions which helped to significantly improve the manuscript.

REFERENCES

Alabi, A. B., Forbes, D. A., Romanowsky, A. J. et al.: 2016, *Mon. Not. R. Astron. Soc.*, **460**, 3838.
Alabi, A. B., Forbes, D. A., Romanowsky, A. J. et al.: 2017, *Mon. Not. R. Astron. Soc.*, **468**, 3949.
Arnold, J. A., Romanowsky, A. J., Brodie, J. P. et al.: 2014, *Astrophys. J.*, **791**(2), 80.
Bekenstein, J.: 2004, *Phys. Rev. D*, **70**, 083509.
Bell, E. F. and de Jong, R. S.: 2001, *Astrophys. J.*, **550**, 212.
Bertin, G., Ciotti, L. and Del Principe, L.: 2002, *Astron. Astrophys.*, **386**, 149.
Binney, J. J. and Tremaine, S.: 2008, Galactic Dynamics, Second Edition, Princeton Univ. Press, Princeton.
Binney J. J. and Mamon, G.: 1982, *Mon. Not. R. Astron. Soc.*, **200**, 361.
Bruzual, G. and Charlot, S.: 2003, *Mon. Not. R. Astron. Soc.*, **344**, 1000.
Cappellari, M.: 2016, *Annu. Rev. Astron. Astrophys.*, **54**, 597.
Cappellari, M., Bacon, R., Bureau, M. et al.: 2006, *Mon. Not. R. Astron. Soc.*, **366**, 1126.
Casuso, E., Vazdekis, A., Peletier, R. F. and Beckman, J. E.: 1996, *Astrophys. J.*, **458**, 533.
Deason, A. J., Belokurov, V., Evans, N. W. and McCarthy, I. G.: 2012, *Astrophys. J.*, **748**(1), 2.
Debattista, V. P., Corsini, E. M. and Aguerri, J. A. L.: 2002, *Mon. Not. R. Astron. Soc.*, **332**, 65.
Famaey, B. and Binney, J.: 2005, *Mon. Not. R. Astron. Soc.*, **363**, 603.
Famaey, B., Bruneton, J.-P. and Zhao, H. S.: 2007, *Mon. Not. R. Astron. Soc.*, **377**, L79.
Fioc, M. and Rocca-Volmerange, B.: 1997, *Astron. Astrophys.*, **326**, 550.
Forbes, D. A., Sinpetru, L., Savorgnan, G., Romanowsky, A. J., Usher, C. and Brodie, J.: 2017a, *Mon. Not. R. Astron. Soc.*, **464**(4), 4611.
Forbes, D. A., Alabi, A., Brodie, J. P. et al.: 2017b, *Astron. J.*, **153**(3), 114.
Genzel, R., Förster Schreiber, N. M., Übler, H. et al.: 2017, *Nature*, **543**(7645), 397.
Gerhard, O.: 1993, *Mon. Not. R. Astron. Soc.*, **265**, 213.
Into, T. and Portinari, L.: 2013, *Mon. Not. R. Astron. Soc.*, **430**, 2715.
Joanes, D. N. and Gill, C. A.: 1998, *The Statistician*, **47**, 183.
Kroupa, P.: 1998, *ASP Conference Series*, **134**, 483.
Kuntschner, H., Emsellem, E., Bacon, R. et al.: 2010, *Mon. Not. R. Astron. Soc.*, **408**, 97.
Mamon, G. A. and Łokas, E. L.: 2005, *Mon. Not. R. Astron. Soc.*, **362**, 95.

Napolitano, N. R., Romanowsky, A. J., Capaccioli, M. et al.: 2011, *Mon. Not. R. Astron. Soc.*, **411**, 2035.
Navarro, J. F., Frenk, C. S. and White, S. D. M.: 1997, *Astrophys. J.*, **490**, 493.
Pota, V., Forbes, D. A., Romanowsky, A. J. et al.: 2013, *Mon. Not. R. Astron. Soc.*, **428**, 389.
Poulain, P. and Nieto, J. L.: 1994, *Astron. Astrophys. Suppl.*, **103**, 573.
Romanowsky, A. J., Douglas, N. G., Arnaboldi, M., Kuijken, K., Merrifield, M. R., Napolitano, N. R., Capaccioli, M. and Freeman, K. C.: 2003, *Science*, **5640**, 1696.
Romanowsky, A. J., Strader, J., Spitler, L. R., Johnson, R., Brodie, J. P., Forbes, D. A. and Ponman, T.: 2009, *Astron. J.*, **137**, 4956.
Samurović, S.: 2007, *Publ. Astron. Obs. Belgrade*, **81**, 1.
Samurović, S.: 2012, *Astron. Astrophys.*, **541**, A138.
Samurović, S.: 2014, *Astron. Astrophys.*, **570**, A132.
Samurović, S.: 2016, *Serb. Astron. J.*, **192**, 9.
Samurović, S. and Danziger, I. J.: 2005, *Mon. Not. R. Astron. Soc.*, **363**, 769.
Samurović, S. and Ćirković M. M.: 2008, *Astron. Astrophys.*, **488**, 873.
Samurović, S., Vudragović, A., Jovanović, M. and Ćirković, M. M.: 2014, *Serb. Astron. J.*, **188**, 29.
Sanders, R. H.: 2010, The Dark Matter Problem, Cambridge Univ. Press, Cambridge.
Sanders, R. H. and McGaugh, S.: 2002, *Annu. Rev. Astron. Astrophys.*, **40**, 263.
van de Sande, J., Bland-Hawthorn, J., Fogarty, L. M. R. et al.: 2017, *Astrophys. J.*, **835**(1), 104.
Vudragović, A., Samurović, S. and Jovanović, M.: 2016, *Astron. Astrophys.*, **593**, A40.

ДИНАМИЧКИ МОДЕЛИ ДВЕ СОЧИВАСТЕ ГАЛАКСИЈЕ: NGC 1023 И NGC 4526

S. Samurović

Astronomical Observatory, Volgina 7, 11060 Belgrade 38, Serbia
E–mail: *srdjan@aob.rs*

УДК 524.7 NGC1023, NGC4526
Оригинални научни рад

У раду се анализирају кинематика и динамика две сочивасте галаксије које поседују глобуларна јата у свом саставу која су удаљенија од седам ефективних радијуса од њихових центара. Анализиране су две блиске сочивасте галаксије, NGC 1023 и NGC 4526 користећи њихова глобуларна јата. Израчунали смо кинематичке параметре обе галаксије и искористили их у динамичком моделирању заснованом на решавању Џинсове једначине. Џинсова једначина решавана је у њутновској апроксимацији по којој маса прати сјај подразумевајући константан однос маса-сјај и такође узимајући у обзир тамни хало у Наваро-Френк-Вајт форми. Пронађено је да, док за прву галаксију NGC 1023 тамна материја није потребна у великим количинама, у другој галаксији, NGC 4526 тамна материја потпуно доминира у њеној укупној маси. У раду се такође користе три различита MOND приступа и пронађено је да док за обе галаксије MOND модели могу да успешно фитују посматрану дисперзију брзина, у случају галаксије NGC 4526 постоји наговештај о додатној, тамној компоненти чак и у оквиру MOND приступа.